THE JOURNAL OF PHYSICAL CHEMISTRY B

ARTICLE

pubs.acs.org/JPCB

Sorting Mechanisms and Communication in Phase-Separating Coupled Monolayers

Moritz Mercker,*[,†] Thomas Richter,[‡] and Dirk Hartmann[†,§]

[†]BioQuant, BQ 0021, INF 267, D-69120 Heidelberg, Germany

[‡]Institute of Applied Mathematics, INF 293, D-69120 Heidelberg, Germany

Supporting Information

ABSTRACT: A continuous model of two coupled monolayers constituting a fluid bilayer membrane is presented. The model is based on the minimization of a membrane free energy considering in both monolayer leaflets two different molecule types, undergoing lateral phase separation. Differences in the mechanical properties of the molecules, such as shape, stiffness, and length are accounted explicitly by the model. In the presented model, coupling between monolayers is realized via an energy-based model depending on the local distance between the two monolayers as well as the lengths of molecules constituting the local monolayer region. We numerically study different passive mechanisms for molecule sorting and correlation across the bilayer induced by first-order mechanical constraints. Here, we focus on three aspects: First, we find that stretching of the two monolayers in the normal direction yields a sorting of molecules according to their length. Furthermore, we show that the length of molecules can be used to synchronize phases across the bilayer membrane. Moreover, we find that generating curvature in one layer (induced by different curvature creating mechanisms) sorts molecules of the other layer according to their shape and stiffness. Many recent experimental data indicate the importance of specific lipid−protein interactions and the role of the bilayer thickness in membrane protein function and sorting. The presented model proposes different mechanisms leading to a colocalization of different components in different monolayers at the same place at the same time.

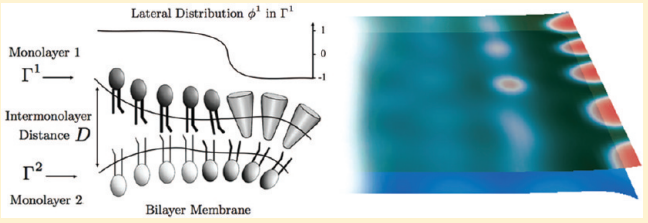

1. INTRODUCTION

Biological membranes define a mechanical boundary of cells as well as of substructures inside cells. They provide environments which are specialized for certain chemical or mechanical processes. Beside mechanical functions membranes typically contain chemically active molecules, such as enzymes. The detailed organization of these molecules is critical for the function of the biological system itself.

The main component of a membrane is the lipid molecule. In water, these lipids form a bilayer structure consisting of two lipid monolayers (see Figure 1). On the one hand, with application of deformations normal to the bilayer, it behaves like an elastic body. On the other hand, the lateral behavior in each monolayer can be compared to a two-dimensional (2D) fluid, since molecules can move freely in lateral direction of the membrane. This ambivalent characteristic of biological membranes has been first described in the "fluid mosaic" model.[1] In vivo, biological membranes are composed of many different molecule species, and the distribution of the species can differ distinctly between the outer and inner layer.[2] The detailed concerted organization of molecules within the bilayer is crucial for any biological function of the system. It has been shown that the length of membrane components and membrane thickness,[3] their stiffness,[4] their shape and structure,[5] as well as lateral phase separation[6] play a major role in membrane organization. Furthermore, experimental results highlight the strong influence of interactions between the monolayers on membrane organization. Differences in the composition of the two monolayers can induce changes in the bilayer shape as well as phase-dependent transversal organization.[7,8] However, the exact mechanisms leading to an appropriate organization remain unknown. One possibility are passive dynamical flows driven by mechanical forces, since the properties of the molecular membrane components directly influence the local mechanical properties of the membrane.

By avoidance of general experimental problems such as unmanageable complexity and the limits of microscopy, various theoretical membrane model systems have been developed in the past.[9] Fully atomistic up to coarse-grained molecular dynamical approaches are available to investigate different magnitudes of the molecular scale. However, they are generally restricted to small spatial and temporal scales. To investigate larger scales various continuous approaches for lateral heterogeneous membranes, mainly based on the Helfrich-functional,[10] have been developed assuming a description of the membrane as a curved 2-D surface.[11−15] But they mainly treat the membrane as one layer. Studies explicitly considering a separate inner and outer monolayer are either restricted to

Received: May 4, 2011
Revised: August 29, 2011
Published: September 02, 2011

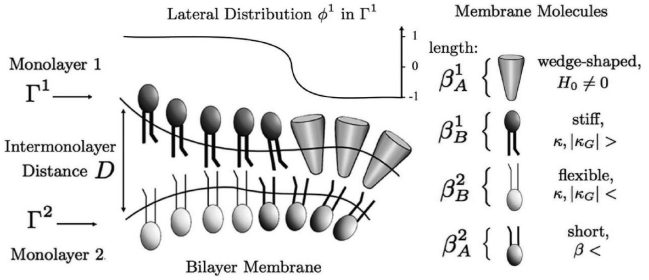

Figure 1. Continuous bilayer model: Each monolayer is represented by a surface Γ^i and its lateral composition by an order parameter ϕ^i, $i \in \{1,2\}$. Molecule properties are outlined on the right-hand side. Intermonolayer distance is measured by D, not necessarily coinciding with the optimal distance $a = (\beta_B^1 + \beta_B^2)/2$, as shown on the left-hand side.

lateral homogeneous membranes[16,17] or deformations have not been considered.[18,19]

In this work, we present a continuous mathematical model of a fluid bilayer membrane, consisting of two explicitly given coupled monolayers. Each monolayer consists of two different lateral phase separating components. The model accounts for differences in the length, stiffness and shape of the molecules (described by macroscopic elastic moduli), as well as a boundary energy between separating phases. We numerically study how the interplay of membrane shape, thickness, lateral, and transversal organization is affected by the exact composition of the membrane as well as the exact dependence on the mechanical properties of the different membrane components found in the monolayers. The results are discussed in the context of recent experimental results and related biological processes.

2. METHODS

Free Energy Model. In this work, we address a continuous approach to model and simulate the deformations and in-plane organization of lipids and proteins of a lipid bilayer membrane. (For more details on the concepts and notations of differential geometry used in our approach we refer to the work of Nelson[20]) In contrast to previous intermonolayer coupling studies, where a phenomenological coupling constant has been used,[18,21] all observed sorting effects result directly from the following two basic assumptions: (I) the thickness of the bilayer depends on the length of the opposed molecules; (II) different molecular species can vary in their shape, length or stiffness. Furthermore, the model can be explicitly parametrized by the relevant parameters of molecular length and elastic moduli (given in physical units).

For $i \in \{1,2\}$, each monolayer patch is represented by a two-dimensional (2D) surface Γ^i curved in 3D space, depicted by a parametric representation $\vec{X}^i(u_1,u_2)$: $U \rightarrow \Gamma^i \subset \mathbb{R}^3$ with $U = [0,1] \times [0,1]$. The concentration of two components A and B in Γ^i is described by the order parameter $\phi^i: U \rightarrow [-1,1]$. If $\phi^i = -1$ the membrane Γ^i is locally composed to 100% by species B, if $\phi^i = 1$ locally only species A is present. We assume that hydrophobic interactions between the two monolayers mainly take place between opposed molecules, i.e., molecules only interact with the nearest molecules on the other monolayer. The distance between the layers, i.e., between interacting molecules, is given locally by the distance function $D^i: \Gamma^i \rightarrow \Gamma^j$, where D^i maps $X^i \in \Gamma^i$ to $X^j \in \Gamma^j$ such that X^j has minimal distance to X^i. Hence, for each molecule in layer i the function D^i measures the distance to the nearest opposed molecule in the other layer (c.f. Supporting Information available online).

By adoption of a common approach, our model is based on the minimization of the bilayer free energy $F = F^1 + F^2$, where for each monolayer Γ^i ($i = 1,2$) the free energy is given by $F^i = {F_1}^i + {F_2}^i + {F_3}^i$

$$F_1^i = \int_{\Gamma^i} \left(\frac{\kappa^i(\phi^i)}{2} (H^i - H_0^i(\phi^i))^2 + \kappa_G^i(\phi^i) K^i \right) ds^i$$

$$F_2^i = \tilde{\sigma}^i \int_{\Gamma^i} \left(\frac{(\xi^i)^2}{2} (\nabla^{\Gamma^i} \phi^i)^2 + f^i(\phi^i) \right) ds^i$$

$$F_3^i = \frac{\alpha}{2} \int_{\Gamma^i} (D^i(X^i) - a(\phi^i, \phi^j))^2 ds^i$$

Here, superscripts denote the monolayer and subscripts refer to different types of energies/interactions. F_1^i is the bending elastic energy of the membrane,[10] where ds^i is the surface area element. Since curvatures in curved 2D surfaces are well described by two quantities, the mean curvature H and the Gaussian curvature K for each monolayer i the energy F_1^i depends on H^i and K^i. The spontaneous curvature H_0^i represents the preferred mean curvature in the relaxed state which can be nonzero, if, e.g., molecules are wedge-shaped. The stiffness of monolayer i is represented by the bending rigidity κ^i and the Gaussian rigidity κ_G^i; the latter is often referred to as the saddle−splay modulus. In the case of homogeneous monolayers, the elastic moduli κ^i, κ_G^i, and H_0 are taken as constants, whereas K^i and H^i depend on the local geometry of the monolayers. In the presented study, both monolayers consist of different molecule species. Since different types of membrane molecules can display different mechanical properties, elastic moduli are assumed to depend on the local composition of the monolayers, described by ϕ^i. We assume that elastic moduli are linear functions of ϕ^i, i.e., $\kappa^i(\phi^i) = (\kappa_A^i + \kappa_B^i)/2 + ((\kappa_A^i - \kappa_B^i)/2)\phi^i$, where κ_A^i and κ_B^i are the bending rigidities of the molecular species A and B in Γ^i. H_0^i and κ_G^i are defined analogously.

F_2^i is the so-called Cahn−Hilliard energy describing lateral phase separation of the two species A and B.[22] This energy contribution has been included, since lateral demixing seems to be a fundamental process underlying spatial organization in biological membranes.[6,23] In this energy part, ξ^i is a phase transition length; $\sigma^i = \tilde{\sigma}^i \cdot \xi^i$ represents the line tension (acting mainly on domain boundaries in order to shorten them), ∇^{Γ^i} the surface gradient, and $f^i = (9/32)((\phi^i)^2 - 1)^2$ a double well potential, causing the separation into two phases.

Finally, the free energy ${F_3}^i$ elastically penalizes deviations of the intermonolayer distance from an "optimal bilayer thickness," described by the function $a = a(\phi^i,\phi^j)$ and weighted by α. The optimal thickness of a bilayer is mainly determined by the length of opposite molecules.[24,25] The physical origin of F_3^i is related to the "hydrophobic effect," i.e., an interaction force causing the clustering of hydrophobic units in water.[26] In the case of lipid bilayers, it is based on strong attractions between hydrophilic parts of membrane molecules and water, partly stabilized by hydrophobic forces.[27] Furthermore, we assume that different molecule lengths and deviations from this optimal thickness primarily change the average distance between opposed molecule heads (leading, e.g., to entropic changes).[28−30] Additionally,

the lengths shall not significantly influence the molecules equilibrium area per molecule-head presented to the water, since head groups try to keep a closed surface. Hence, bilayer thickness fluctuations do not contradict the assumed lateral area incompressibility of the two monolayer leaflets. (Also incompressibility is considered separately for each monolayer—in contrast to previous studies where the bilayer midplane is assumed to be incompressible.[31,32]) It has been early shown that the thickness of a lipid bilayer varies linearly with the length of membrane molecules.[24] Hence, we assume that the bilayer optimal thickness function depends linearly on the average length of locally opposed molecules: if β^i_A and β^i_B represent the lengths of the molecules A and B in Γ^i, the local average molecule length in Γ^i is given by $\beta^i(\phi^i) := (\beta^i_A + \beta^i_B)/(2) + ((\beta^i_A - \beta^i_B)/2)\phi^i$. Since the bilayer optimal thickness function measures the distance between the midplanes of the two monolayer leaflets (c.f. Figure 1) it is given by the average of the opposite molecule lengths, i.e., $a := (\beta^i(\phi^i) + \beta^j(\phi^j))/2$.

Given a certain state of the membrane system, the system evolves in the direction of the steepest decent of the free bilayer energy. By assumption of an overdamped motion, which is typically a valid assumption for molecular systems, dynamics of the deformation $\vec{X}^i$ in $U \times [0,T)$ are given by the following gradient flow under the constraint of a strong local area incompressibility of each monolayer leaflet (considered separately)

$$\partial_t[\vec{X}^i] = -L_{X^i}\frac{\delta}{\delta \vec{X}^i}[F^i + \int_{\Gamma^i}\gamma^i ds^i] \quad (1)$$

$$\partial_t[\sqrt{g^i}] = 0 \quad (2)$$

for i = 1,2. Hence, an evolution of each monolayer takes place in order to minimize the free energy, which depends in turn on local curvatures, compositions and the distance to the other monolayer. L_{Xi} is a kinetic coefficient (scaling inversely with the viscosity of the surrounding medium), $(\delta/\delta\vec{X}^i)[F^i]$ denotes the variation of F^i with respect to $\vec{X}^i$ (c.f. Supporting Information available online), γ^i is a local Lagrange multiplier,[33] and g is the determinant of the first metric tensor.[20] Since the surface measure of a curved surface is defined by $ds = g^{1/2}d^2u$, eq 2 represents the local surface incompressibility.

Assuming local mass conservation, lateral dynamics of the two species A and B are determined by the lateral continuity equation $d_t\phi + \nabla^\Gamma\vec{j} = 0$. (For convenience we neglect superscripts for the moment.) Since we work within a Lagrangian point of view, $d/d_t\phi$ can be evaluated directly. Adopting an Eulerian point of view one has to consider $(d/dt)\phi = \nabla^\Gamma[\phi]\partial_t\vec{X} + \partial_t\phi$, i.e., the convection of ϕ with the deforming surface has to be considered. The flux is proportional to the lateral gradient of the chemical potential $\mu(u_1,u_2)$, i.e., $\vec{j} = -L_\phi\nabla^\Gamma\mu$. μ is determined by the variation of the free energy F with respect to ϕ. Thus it holds $\mu = (\delta/\delta\phi)[F]$. The mobility L_ϕ is assumed to be constant (scaling inversely with the viscosity of the membrane—the corresponding diffusion coefficient is given by $D = L_\phi\tilde{\sigma}$). Altogether, we have the following dynamical equation for ϕ in $U \times [0,T)$ considering both monolayers separately

$$d_t[\phi^i] = L_{\phi^i}\Delta^{\Gamma^i}\left[\frac{\delta}{\delta\phi^i}[F]\right] \quad (3)$$

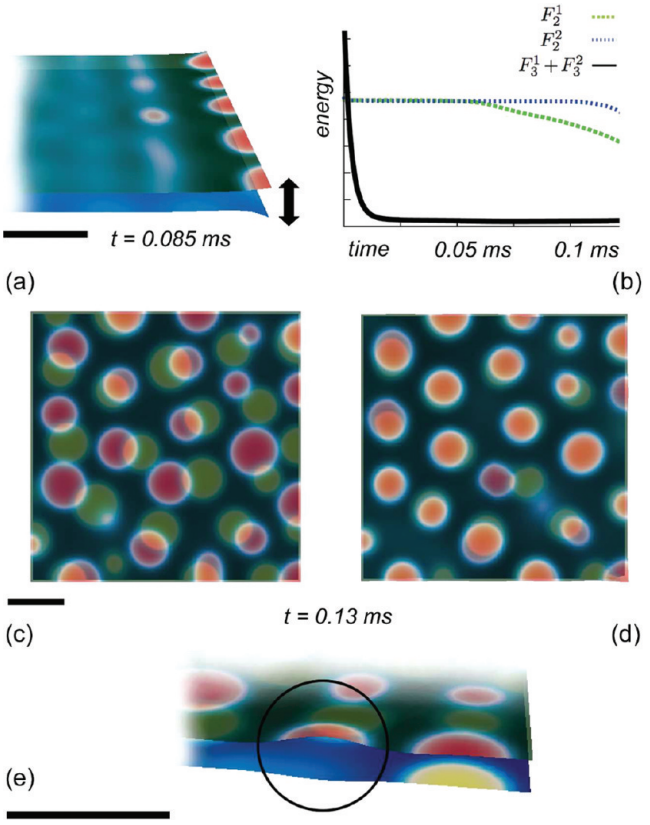

Figure 2. Influence of molecule lengths on intermonolayer coupling. Red and green correspond to high local concentrations of species A and B in the upper monolayer; yellow and blue correspond to local high concentrations of species A and B in the lower monolayer, respectively. (a) Stretching of the two monolayers in the normal direction leads to a sorting of long molecules to the stretched area in Γ^1, whereas the molecules in Γ^2 have the same length. (b) Corresponding decay of different parts of the free energy F. (d) Long molecules are sorted opposite to short molecules, whereas all molecules in (c) have the same length. (e) Detailed view of (d); nonsynchronized domains (black circle) induce curvatures in both layers. (Scale bars: 10 nm).

for i = 1,2 (c.f. also Supporting Information available online).

Numerical Methods and Parameters. By use of the outlined macroscopic modeling approach, we investigate the effect of molecule length variations and curvature modulated sorting. To do so, we numerically approximate eqs 1−3 to study systematically deformations and lateral dynamics of two coupled monolayers constituting a lipid bilayer. For spatial discretization we use a mixed finite element approach related to Barrett[34] and Elliot,[35] where the surface of each monolayer is discretized using a quadrangular grid with M^i = 4096 grid points, i.e., in total 8192 grid points. To keep the complexity controlled, we do not apply any lateral tension and impose Dirichlet-zero boundary conditions for X^i_1 and X^i_2 as well as natural boundary conditions. For time discretization we use an adaptive semi-implicit Euler scheme. As not otherwise stated, we use in both monolayers stochastic initial conditions, representing the disordered and homogeneous mixture of molecules at high temperatures (further initial conditions are detailed in the Supporting Information available online). If not otherwise stated, we use the following set of parameters: $\kappa^i(\phi^i) \equiv 20\ k_BT$, $\kappa^i_G(\phi^i) \equiv -10\ k_BT$, $H^i_0(\phi^i) \equiv 0\ \mathrm{nm}^{-1}$, $\tilde{\sigma}^i = 1400\ k_BT\ \mu\mathrm{m}^{-2}$, $\xi = 0.8$ nm, $\alpha^i = 9.6 \times 10^7\ k_BT\ \mu\mathrm{m}^{-4}$,

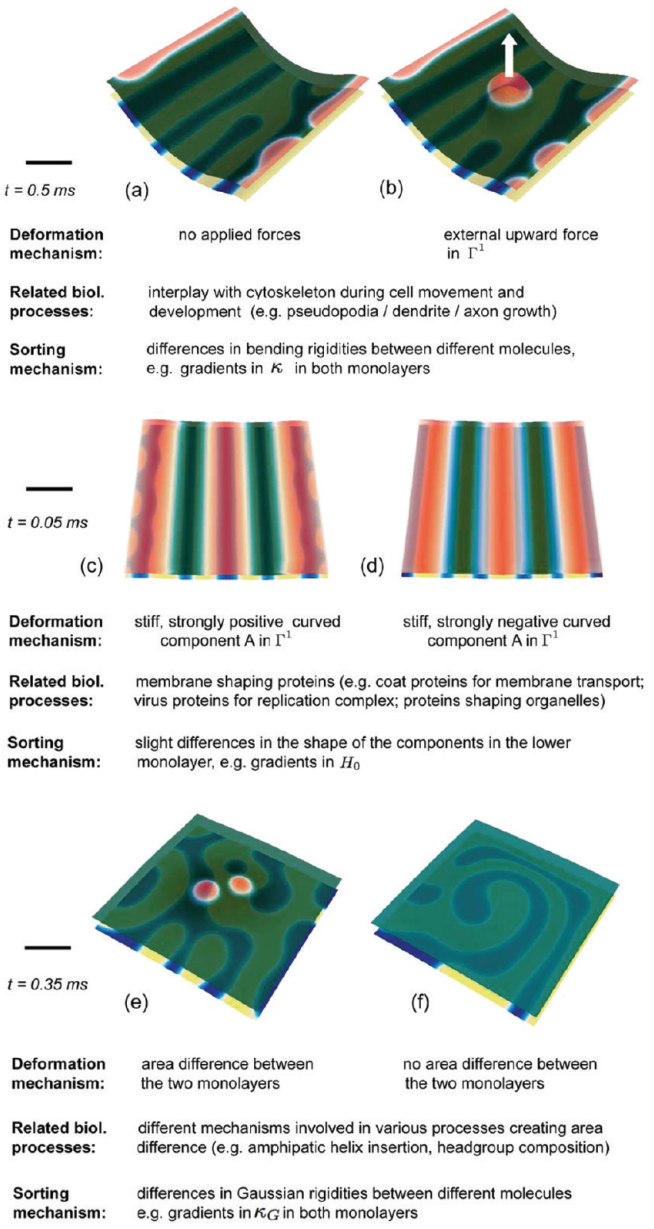

Figure 3. Curvature-mediated intermonolayer coupling. Red and green correspond to high local concentrations of species A and B in the upper monolayer; yellow and blue correspond to high local concentrations of species A and B in the lower monolayer, respectively. Curvature-mediated phase separation in each comparative simulation is driven by gradients in one elastic modulus. Local curvatures have been generated by applying an upward force to Γ^1 in (b) contrary to (a), by choosing contrary spontaneous curvatures $H_0^1(1)$ in (c) and (d) and by introducing a nontrivial global area difference in (e) contrary to (f). (Scale bars: 10 nm).

$L_{X^i} = 6.25 \times 10^{-11}\,\mu\mathrm{m}^4\,\mathrm{s}^{-1}\,(k_\mathrm{B}T)^{-1}$, $L_{\phi^i} = 3.12 \times 10^{-5}\,\mu\mathrm{m}^4\,\mathrm{s}^{-1}\,(k_\mathrm{B}T)^{-1}$, $a \equiv 2.5$ nm, for $i \in \{1,2\}$. This parameter set corresponds to the molecular diffusion coefficient $D = \tilde{\sigma}^i = 1.1 \times 10^{-10}\,\mathrm{cm}^2\,\mathrm{s}^{-1}$ and the line tension $\sigma^i = \tilde{\sigma}^i\tilde{\xi} = 1.15\,k_\mathrm{B}T\,\mu\mathrm{m}^{-1}$. (Odd numbers result from the conversion of abstract nondimenzionalized model parameters into physical values.) Most of the parameters have been already characterized by experimental means and these are of the same order of magnitude as the values used here.[36−39]

3. RESULTS

Membrane Organization Induced by Varying Molecular Lengths. Motivated by many experimental studies indicating the importance of interactions of lipids and membrane proteins due to varying molecule sizes,[3] we investigate the impact of molecule size on lateral membrane organization, i.e., molecular sorting. To do so, we study two coupled monolayers differing from each other with respect to their composition of molecules with different lengths (c.f. Figure 2). (For all corresponding simulations we use constant elastic moduli.)

In Figure 2a, we artificially stretch two monolayers on one side apart by an appropriate choice of boundary conditions in the normal direction mimicking big membrane spanning proteins. In Γ^1 we consider molecules with two different lengths $\beta_\mathrm{A}^1 = 3$ nm and $\beta_\mathrm{B}^1 = 2$ nm, and in Γ^2 two species with the same lengths $\beta_\mathrm{A}^2 = \beta_\mathrm{B}^2 = 2.5$ nm. During the simulation, we observe a distance relaxation between the monolayers combined with a distance-dependent lateral sorting in Γ^1 and a distance-independent sorting in Γ^2. In Γ^1 the longer molecules ϕ_A separate with a strong preference for the region close to the boundary where the normal stretch is applied, whereas in Γ^2 no special preference can be observed, as expected. Furthermore, the Cahn−Hilliard energy F_2^1 decays faster than F_2^2 (c.f. Figure 2b), i.e., different molecular lengths do not only lead to an accumulation at specific places but also enhances the speed of the sorting process (c.f. Figure 2b).

Above we have considered one layer with molecules of the same length and one layer with molecules of different lengths. Now let us consider the following two different scenarios: in (c) $\beta_\mathrm{A}^1 = \beta_\mathrm{B}^1 = \beta_\mathrm{A}^2 = \beta_\mathrm{B}^2 = 2.5$ nm and in (d) $\beta_\mathrm{A}^1 = \beta_\mathrm{B}^2 = 4$ nm and $\beta_\mathrm{A}^1 = \beta_\mathrm{B}^2 = 1$ nm. In both cases no artificial stretching has been applied. We observe that different molecule lengths induce a spatial phase synchronization between the monolayers: Long molecules of one layer are sorted to short molecules of the other layer, causing (in the given ratio of components) a bilayer of homogeneous thickness.

Membrane Organization Induced by Curvature Modulated Intermonolayer Coupling. Inspired by the richness of curvature generating mechanisms[40] and recent experimental evidence for curvature modulated lateral sorting,[4,41] we further investigate the interplay of curvature and lateral/transversal sorting between two coupled monolayers. Corresponding results are presented in Figure 3. Previous theoretical studies typically have used a phenomenological coupling constant to describe curvature modulated sorting.[12,42−45] Whereas the effects observed here result directly from first physical principles, namely, from the assumption that different molecules can vary in their shape and stiffness.

We demonstrate that deformations in one monolayer induced by different mechanisms (identified by experiments) influence the chemical distribution in both layers, if the molecules vary in stiffness or shape. The latter is modeled via differences in macroscopic elastic moduli, e.g., the bending rigidity κ, the Gaussian rigidity κ_G, and the local spontaneous curvature H_0. For all corresponding simulations we use constant molecule lengths.

Figure 3 shows the interaction of two components A and B in both layers with different bending moduli leading to a sorting of molecules. In the following, we will study the detailed interplay between lateral sorting and curvature generating mechanisms. By adoption of the most basic curvature generating mechanisms in

biological membranes,[5] local curvatures are induced via different mechanisms:

In Figure 3b contrary to part a we apply a constant circular upward force in the middle of Γ^1, corresponding, e.g., to tubules applying a force via motor proteins pushing the membrane.[46]

In parts c and d of Figure 3, we simulate stable clusters of stiff shaping membrane proteins in Γ^1 choosing $\phi_0^1 = \sin(5\pi u_1)$, $L_\phi^1 = 0$, and $\kappa^1(1) = 40\ k_BT$ with positive curvature $H_0^1(1) = 0.2\ \mathrm{nm}^{-1}$ in (c) as well as negative curvature $H_0^1(1) = -0.2\ \mathrm{nm}^{-1}$ in (d). A corresponding example in biological membranes is, e.g., the scaffolding mechanism: a huge rigid protein or a protein domain that has an intrinsic curvature bends the membrane beneath it, but lateral dynamics of lipids are possible in at least one monolayer.[47]

In Figure 3e, as opposed to part f, the global area A_2 of Γ^1 differs from A_1, which has been assumed as a curvature-generation mechanism[48] and is proven to be a frequent mechanism in biological membranes—a prominent example is the amphipatic helix insertion.[49]

In all simulations shown in Figure 3, lateral sorting is induced choosing differences in stiffness or shape of different membrane components, expressed by differences among the species A and B in one of the macroscopic elastic moduli: the bending rigidity κ, the spontaneous curvature H_0, or the Gaussian rigidity κ_G. In (a−b) we have set $\kappa^i(1) = 19.9\ k_BT$, but $\kappa^i(-1) = 20\ k_BT$; in (c−d) $H_0^2(1) = -5 \times 10^{-3}\ \mathrm{nm}^{-1}$, but $H_0^2(-1) = 5 \times 10^{-3}\ \mathrm{nm}^{-1}$, and in (e−f) $\kappa_G^i(1) = -8.88\ k_BT$, but $\kappa_G^i(-1) = -10\ k_BT$; $i \in \{1,2\}$.

The exact choice of the inhomogeneous elastic modulus does not depend on the curvature-generating mechanism. For clarity, we have restricted us to selected cases of interplay between curvature generating and lateral sorting mechanisms. One can imagine the rich diversity of possible interplays in real membranes.

4. DISCUSSION

Above we have addressed the following main aspects of membrane organization: sorting due to different molecule lengths, phase synchronization across monolayers, as well as the interplay between curvature generation and lateral sorting mechanisms. The physical interaction and the hereby possible mutual activation or deactivation of different membrane molecules plays a key role in various cellular processes: integral membrane proteins are often activated by special lipid molecules surrounding them.[3] Furthermore, lateral as well as transversal interactions between different membrane proteins play a key role in various biological processes, such as signaling, photosynthesis, and endocytosis.

Membrane Organization Induced by Varying Molecular Lengths. It has been assumed that the thickness of the membrane or rather the hydrophobic mismatch of different components influences these interactions.[50] To investigate the effect of molecule length on lateral sorting, we have stretched the distance between the two monolayers of the bilayer membrane at one edge, corresponding in vivo, e.g., to the effects mediated by membrane spanning proteins.[51] We have observed that this thickness mismatch can induce phase separation and sorts molecules according to their length: Long molecules aggregate very early in time close to the stretched region (c.f. parts a and b of Figure 2). These observations of an aggregation of equally sized molecules in order to minimize the hydrophobic mismatch are in accordance with the assumptions of Killian,[50] molecular dynamical studies on small scales,[52−55] as well as experimental results.[56] We should mention that the effect of molecule tilt is not considered within our model.

Furthermore and in accordance with recent molecular dynamical results[52] our simulations have revealed that the length of membrane molecules can be used to induce a synchronization of phases across the bilayer membrane (c.f. parts c−e of Figure 2). This synchronization is the result of a combination of two distinct processes: On the one hand the monolayer bending rigidity prevents the layers from small scale spatial curvature fluctuations. These fluctuations become more obvious looking at regions where the synchronization does not take place ((e) black circle) and induce curvatures in both layers. On the other hand the molecule dynamics drive components in regions where they "fit the bilayer thickness." The same mechanism but on the scale of single molecules has been proposed by Adachi et al.,[57] investigating interdigitated phases of phospholipids and alcohols.

Recent studies have proposed different mechanisms for hydrophobic mismatch dependent sorting and interleaflet coupling.[3,58−60] These studies have been mainly focused on energetic and entropic contributions of local compression or stretching of hydrophobic lipid tails. The mechanism presented in this study could explain how cells achieve lateral and transversal sorting of components which do not exhibit "flexible" parts, such as membrane proteins. In vivo, the observed sorting could constitute mechanisms in cells to assemble membrane proteins with certain chemical or mechanical properties close to each other or to other membrane spanning or compressing protein complexes, found in various cell processes such as signaling.

Membrane Organization Induced by Curvature-Modulated Intermonolayer Coupling. So far we have considered the influence of different molecule lengths on lateral sorting. Let us now focus on the interplay between lateral sorting and curvature generating mechanisms in coupled monolayers. Cellular membranes are strikingly dynamic structures changing their shape in various processes such as movement, division, during neuronal development, and vesicle traffic. Some of the main mechanism hereby are deformations due to external forces such as the actin cytoskeleton, scaffolding by peripheral membrane proteins and area differences between the two monolayers, e.g., induced by asymmetric lipid distributions.[5,47] Although the shaping mechanisms themselves are well characterized, the mechanisms for a concerted organization of different components in different monolayers during the deformation process is poorly understood.

In this study, to our knowledge, for the first time the interplay of different membrane curvature generating mechanisms with different lateral sorting mechanisms in both monolayers is investigated (c.f. Figure 3). Motivated by experimental data,[4,41] our results clearly show that differences among molecular species in each of the three macroscopic mechanical moduli, the bending rigidity κ, the Gaussian rigidity κ_G (both reflecting the molecule stiffness), and the spontaneous curvature H_0 (reflecting the molecule shape) are sufficient for curvature dependent lateral sorting. These results highlight the multitude and complexity of different shapes and lateral patterns that can occur in biological membranes—simply as a result of passive flows of molecules that differ in their first-order mechanical properties. In vivo, curvature mediated intermonolayer coupling could be an important

selection mechanism for the cell: while certain components produce local curvatures (for example shaping proteins or the cytoskeleton) other components can be included in these regions simply due to their mechanical properties by the sorting mechanisms outlined above. This could explain how different structural and catalytic components are getting locally concentrated, e.g., in virus induced deformations.[61]

5. CONCLUSIONS

In this article, a continuous model of two coupled monolayers consisting of different molecule species has been studied. Coupling of the layers has been achieved by an elastic intermonolayer−distance energy term, depending on the molecule lengths in the two opposed layers. We have shown that both the curvature of one layer as well as the distance to the other layer can influence the chemistry distribution in the other layer: our results show that phase separation and local accumulation of membrane components in stretched regions can be induced by a mismatch between molecule size and bilayer thickness. Furthermore, our results suggest that this thickness mismatch effect can serve as a mechanism to synchronize phases across the bilayer membrane. Additionally, we have studied the interplay between membrane curvature and lateral sorting of molecules, showing that differences in stiffness and shape of molecules lead to various possible scenarios of interplays between lateral sorting and local curvature generating mechanisms.

Various basic cellular processes such as budding, signaling, and sorting require the existence of distinctly shaped and composed membrane systems presuming a high magnitude of lateral and transversal membrane organization. The mechanisms presented here could constitute basal mechanisms for these processes, i.e., passive flows of molecules with differences in length, shape, and stiffness lead to a multitude of different lateral and transversal organized membrane shapes.

■ ASSOCIATED CONTENT

Supporting Information. Further details on the model as well as initial conditions used in the simulations. This material is available free of charge via the Internet at http://pubs.acs.org/.

■ AUTHOR INFORMATION

Corresponding Author

*E-mail: moritz.mercker@bioquant.uni-heidelberg.de. Phone: +49-6221-5451336. Fax: +49-6221-548996.

Present Addresses

§Siemens AG, Corporate Technology, D-80200 Munich, Germany

■ ACKNOWLEDGMENT

The authors greatly thank W. Jäger, M. Weiss, and A. Marciniak-Czochra for scientific support. We acknowledge financial support of the ViroQuant Project (German FORSYS initiative) and the Heidelberg Academy of Sciences and Humanities.

■ REFERENCES

(1) Singer, S. J.; Nicolson, G. L. *Science* **1972**, *175*, 720–731.
(2) van Meer, G.; Voelker, D. R.; Feigenson, G. W. *Nat. Rev. Mol. Cell Biol.* **2008**, *9*, 112–124.
(3) Lee, A. G. *Biochim. Biophys. Acta* **2004**, *1666*, 62–87.
(4) Parthasarathy, R.; Yu, C.; Groves, J. *Langmuir* **2006**, *22*, 5095–5099.
(5) McMahon, H. T.; Gallop, J. L. *Nature* **2005**, *438*, 590–596.
(6) Baumgart, T.; Hess, S. T.; Webb, W. W. *Nature* **2003**, *425*, 821–824.
(7) Holopainen, J. M.; Angelova, M. I.; Kinnunen, P. K. *Biophys. J.* **2000**, *78*, 830–838.
(8) Collins, M. D.; Keller, S. L. *Proc. Natl. Acad. Sci. U.S.A.* **2008**, *105*, 124–128.
(9) Chan, Y.-H. M.; Boxer, S. G. *Curr. Opin. Chem. Biol.* **2007**, *11*, 581–587.
(10) Helfrich, W. *Z. Naturforsch.* **1973**, *28*, 693–703.
(11) Jülicher, F.; Lipowsky, R. *Phys. Rev. Lett.* **1993**, *70*, 2964–2967.
(12) Taniguchi, T. *Phys. Rev. Lett.* **1996**, *76*, 4444–4447.
(13) Lowengrub, J. S.; Rätz, A.; Voigt, A. *Phys. Rev. E* **2009**, *79*, 031926.
(14) Minami, A.; Yamada, K. *Eur. Phys. J. E* **2007**, *23*, 367–374.
(15) Wang, X.; Du, Q. *J. Math. Biol.* **2008**, *56*, 347–371.
(16) Lim, G.; Wortis, M.; Mukhopadhyay, R. *Proc. Natl. Acad. Sci. U. S.A.* **2002**, *99*, 16766–16769.
(17) Yeung, A. *Mechanics of Inter-Monolayer Coupling in Fluid Surfactant Bilayers*. Ph.D. thesis, University of British Columbia, 1994
(18) Wagner, A. J.; Loew, S.; May, S. *Biophys. J.* **2007**, *93*, 4268–4277.
(19) Allender, D. W.; Schick, M. *Biophys. J.* **2006**, *91*, 2928–2935.
(20) David, F. In *Statistical Mechanics of Membranes and Surfaces*; Nelson, D., Weinberg, S., Piran, T., Eds.; World Scientific Press: Singapore, 2004.
(21) Hansen, P. L.; Miao, L.; Ipsen, J. H. *Phys. Rev. E* **1998**, *58* (2), 2311–2324.
(22) Cahn, J.; Hilliard, J. *J. Chem. Phys.* **1958**, *28* (2), 258–267.
(23) Parthasarathy, R.; Groves, J. *Soft Matter* **2007**, *3*, 24–33.
(24) Lewis, B. A.; Engelman, D. M. *J. Mol. Biol.* **1983**, *166*, 211–217.
(25) Rawicz, W.; Olbrich, K. C.; McIntosh, T.; Needham, D.; Evans, E. *Biophys. J.* **2000**, *79*, 328–339.
(26) Chandler, D. *Nature* **2005**, *437*, 640–647.
(27) Safran, S. *Statistical Thermodynamics of Surfaces*; Addison-Wesley: Reading., MA, 1994; Chapters 1−3.
(28) Illya, G.; Lipowsky, R.; Shillcock, J. C. *J. Chem. Phys.* **2006**, *125*, 114710.
(29) Szleifer, I.; Kramer, D.; Ben-Shaul, A.; Roux, D.; Gelbart, M. *Phys. Rev. Lett.* **1988**, *60*, 1966–1969.
(30) Schmidt, U.; Guigas, G.; Weiss, M. *Phys. Rev. Lett.* **2008**, *101*, 128104.
(31) Seifert, U.; Berndl, K.; Lipowsky, R. *Phys. Rev. A* **1991**, *44*, 1182–1202.
(32) Miao, L.; Seifert, U.; Wortis, M.; Döbereiner, H. *Phys. Rev. E* **1994**, *49*, 5389–5407.
(33) Foltin, G. *Phys. Rev. E* **1994**, *49*, 5243–5248.
(34) Barrett, J.; Garcke, H.; Nürnberg, R. *SIAM J. Sci. Comp.* **2008**, *31*, 225–253.
(35) Elliott, C.; French, D.; Milner, F. *Numer. Math.* **1989**, *54*, 575–590.
(36) Agrawal, N. J.; Nukpezah, J.; Radhakrishnan, R. *PLoS Comput Biol* **2010**, *6*.
(37) Schwarz, U.; Gompper, G. *Lect. Notes Physics* **2002**, *600*.
(38) Frolov, V. A. J.; Chizmadzhev, Y. A.; Cohen, F. S.; Zimmerberg, J. *Biophys. J.* **2006**, *91*, 189–205.
(39) Sowers, A. E.; Hackenbrock, C. R. *Proc. Natl. Acad. Sci. U.S.A.* **1981**, *78*, 6246–6250.
(40) Shibata, Y.; Hu, J.; Kozlov, M. M.; Rapoport, T. A. *Annu. Rev. Cell Dev. Biol.* **2009**, *25*, 329–354.
(41) Yoon, T.-Y.; Jeong, C.; Lee, S.-W.; Kim, J. H.; Choi, M. C.; Kim, S.-J.; Kim, M. W.; Lee, S.-D. *Nat. Mater.* **2006**, *5*, 281–285.
(42) Allain, J.-M.; Amar, M. B. *Eur. Phys. J. E* **2006**, *20*, 409–420.
(43) Chen, C. M. *Phys. Rev. E* **1999**, *59*, 6192–6195.
(44) Jiang, Y.; Lookman, T.; Saxena, A. *Phys. Rev. E* **2000**, *61*, R57–R60.
(45) Yin, Y.; Lv, C. *J. Biol. Phys.* **2008**, *34*, 591–610.
(46) Roux, A.; Cuvelier, D.; Nassoy, P.; Prost, J.; Bassereau, P.; Goud, B. *EMBO J.* **2005**, *24*, 1537–1545.

(47) Zimmerberg, J.; Kozlov, M. M. *Nat. Rev. Mol. Cell Biol.* **2006**, *7*, 9–19.
(48) Sheetz, M. P.; Singer, S. J. *Proc. Natl. Acad. Sci. U.S.A.* **1974**, *71*, 4457–4461.
(49) Drin, G.; Antonny, B. *FEBS Lett.* **2010**, *584*, 1840–1847.
(50) Killian, J. A. *Biochim. Biophys. Acta* **1998**, *1376*, 401–415.
(51) Duque, D.; Li, X.-J.; Katsov, K.; Schick, M. *J. Chem. Phys.* **2002**, *116*, 10478.
(52) Morozova, D.; Guigas, G.; Weiss, M. *PLoS Comput. Biol. Biol.* **2011**, *7* (6), 1–11.
(53) de Meyer, F. J.-M.; Rodgers, J. M.; Willems, T. F.; Smit, B. *Biophys. J.* **2010**, *99*, 3629–3638.
(54) de Meyer, F. J.-M.; Venturoli, M.; Smit, B. *Biophys. J.* **2008**, *95*, 1851–1865.
(55) Bennun, S. V.; Longo, M. L.; Faller, R. *Langmuir* **2007**, *23*, 12465–12468.
(56) Ivanova, V. P.; Makarov, I. M.; Schäffer, T. E.; Heimburg, T. *Biophys. J.* **2003**, *84*, 2427–2439.
(57) Adachi, T.; Takahashi, H.; Ohki, K.; Hatta, I. *Biophys. J.* **1995**, *68*, 1850–1855.
(58) Collins, M. D. *Biophys. J.* **2008**, *94*, L32–L34.
(59) Fattal, D. R.; Ben-Shaul, A. *Biophys. J.* **1993**, *65*, 1795–1809.
(60) Andersen, O. S.; Koeppe, R. E. *Annu. Rev. Biophys. Biomol. Struct.* **2007**, *36*, 107–130.
(61) Welsch, S.; Miller, S.; Romero-Brey, I.; Merz, A.; Bleck, C.; Walther, P.; Fuller, S.; Antony, C.; Krijnse-Locker, J.; Bartenschlager, R. *Cell Host Microbe* **2009**, *5* (4), 365–375.